Chapter 1

Noise-Free Rapid Approach to Solve Kinetic Equations for Hot Atoms in Fusion Plasmas

Mikhail Tokar

Additional information is available at the end of the chapter

http://dx.doi.org/10.5772/intechopen.76681

Abstract

At the first wall of a fusion reactor, charged plasma particles are recombined into neutral molecules and atoms recycling back into the plasma volume where charge exchange (*cx*) with ions. As a result hot atoms with chaotically directed velocities are generated which can strike and erode the wall. An approach to solve the kinetic equation in integral form for *cx* atoms, being alternative to statistical Monte Carlo methods, has been speeded up by a factor of 50, by applying an approximate pass method to evaluate integrals, involving the ion velocity distribution function. It is applied to two-dimensional transfer of *cx* atoms near the entrance of a duct, guiding to the first mirror for optical observations. The energy spectrum of hot *cx* atoms, escaping into the duct, is calculated and the mirror erosion rate is assessed. Computations are done for a molybdenum first mirror under plasma conditions expected in the fusion reactor DEMO. Kinetic modeling results are compared with those found with a diffusion approximation valid in very cold and dense plasmas. For ducts at the torus outboard a more rigorous kinetic consideration predicts an erosion rate by a factor up to 2 larger than the diffusion approximation.

Keywords: fusion, plasma, neutral, atoms, kinetic equation, numerical solution

1. Introduction

In devices for thermonuclear fusion research, for example, of the Tokamak type, particles of hydrogen isotopes, deuterium and tritium, are in the form of a hot fully ionized plasma [1, 2]. To avoid a destruction of the machine wall, a special region, the so-called scrape-off layer (SOL), is arranged at the plasma edge, where particles stream along the magnetic field to the

special target plates [3]. Normally, it is done by using additional magnetic coils to form a divertor configuration (see **Figure 1a**).

By reaching the divertor target plates, plasma electrons and ions are recombined into neutral atoms and molecules which are finally exhausted from the device by pumps. However, in a future fusion reactor like DEMO [1, 2], only a minor fraction of 1% of neutrals generated at the targets will be pumped out. The rest of them is ionized again in the plasma near the targets. This "recycling" process significantly restrains the parallel plasma flow in the SOL [4]. Therefore, a considerable fraction of plasma particles lost from the plasma core will reach the vessel wall before they are exhausted into the divertor. Plasma fluxes to the wall saturate it with fuel particles in a time much shorter than the discharge duration, and a comparable amount of neutral species will recycle back from the wall into the plasma. Recycling neutrals are not confined by the magnetic field and penetrate at several centimeters into the SOL. Here, charge exchange (*cx*) collisions of them with ions generate atoms of energies much higher than that of primary recycling neutral particles. A noticeable fraction of such secondary *cx* atoms hit the vessel wall and erode it.

Statistical Monte Carlo methods [5] are normally used to model *cx* atoms at the edge of fusion devices. A crucial obstacle to apply these approaches for extensive parameter studies, for example, with the aim to optimize the duct geometry, has too long calculations needed to achieve reasonably small accident errors. This is, however, necessary, for example, to couple neutral parameters with the plasma calculations. In a one-dimensional geometry, an alternative approach, based on iteration procedure to solve the kinetic equation represented in an integral form, has been elaborated decades ago [6]. Being free from statistical noise and

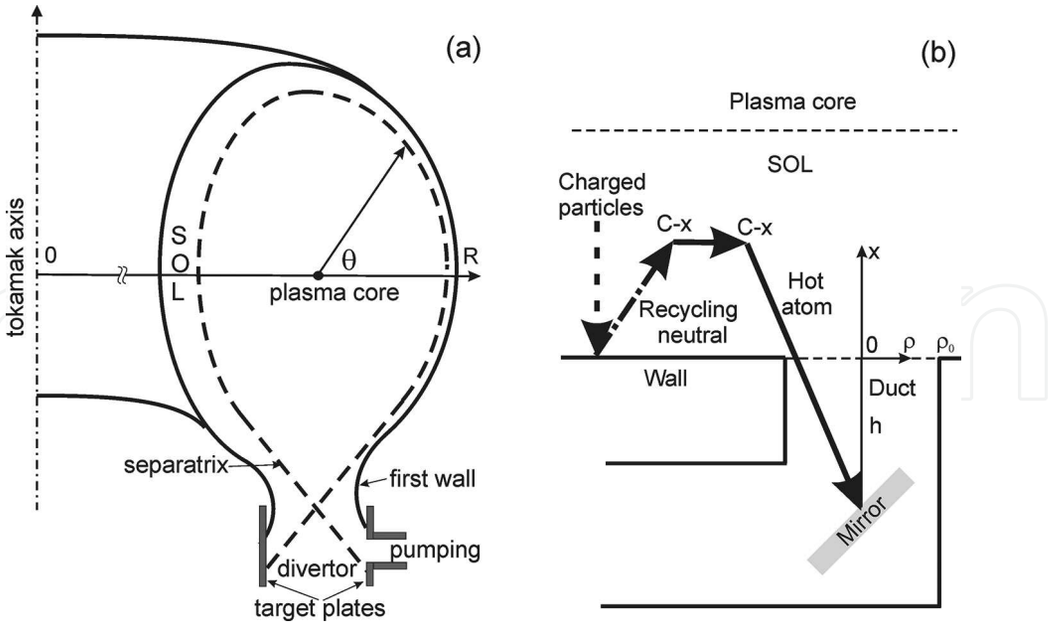

Figure 1. The cross section of toroidally symmetric fusion device of the Tokamak type with the SOL region formed by the presence of a divertor (a) and the processes near the opening in the wall for a duct guiding to a first mirror (b).

permitting the convergence of iterations to the error level defined by the machine accuracy, this method, nonetheless, is also time-consuming. The reason is the necessity to assess integrals in the velocity space from functions involving the ion velocity distribution function, additionally to integrations in the normal space. Recently [4], an approximate pass method has been applied to evaluate these integrals, and the acceleration of kinetic calculations by a factor of 50 has been achieved.

The amendments, outlined above, have allowed to perform calculations of the plasma parameters in the DEMO SOL with *cx* atoms described kinetically, by varying the input parameters, for example, the plasma transport characteristics, in a broad range [4]. In addition the results of these computations have been thoroughly compared with those obtained with *cx* species described in the so-called diffusion approximation. This approximation, often used in diverse edge modeling approaches to save CPU time (see, e.g., [7, 8]), is strictly valid under plasma conditions of low temperature and high density where the time between *cx* collisions of atoms with ions is much smaller than that till their ionization by electrons. Across the DEMO SOL, the plasma density and the temperatures of electrons and ions change, however, by orders of magnitude [4].

The usage of a diffusion approximation for *cx* atoms, generated from species recycling from the wall, becomes especially questionable by considering the situation near an opening in the vessel wall. Such openings will be made in a reactor for diverse purposes, for example, for ducts leading to the first mirrors, collecting light emitted by impurity species in the plasma (see **Figure 1b**). These installations are inaccessible for charged plasma particles, moving mostly along magnetic field lines and penetrating into the duct at a distance of 1 mm. However, hot *cx* atoms, unconfined by the magnetic field, can freely hit and erode these installations. The erosion rate is very sensitive to the energy spectrum of *cx* atoms which can be significantly dependent on the modeling approach. At the position of the duct opening, the inflow of recycling neutrals is actually absent, and the transfer of *cx* atoms has two- or even three-dimensional pattern. By calculating the density of *cx* atoms in the vicinity of a circular opening from a 2D diffusion equation, the erosion rate of a first mirror of Mo has been assessed in [9]. In the present paper, we extend the approaches, elaborated in [4] to model *cx* atoms kinetically in the 1D case, on a 2D geometry.

The results are compared with those of [9]. Although there *cx* atoms have been considered in the diffusion approximation to reduce CPU time, the new approach allows to perform more exact kinetic calculations even by orders of magnitude faster.

2. Basic equations

Although the concept of magnetic fusion is based on the idea that charged particles can be infinitely long confined within closed magnetic surfaces, there are diverse physical mechanisms leading to the losses across these surfaces (see, e.g., [10]). Therefore, electrons and ions escape through the separatrix into the SOL and may reach the first wall of the machine vessel.

Here, these species fast recombine into neutral atoms, with an energy comparable with that of ions. Partly, these atoms escape immediately back into the plasma, and these species are referred as backscattered (*bs*) atoms. The rest transmits the energy to the wall particles and may be bounded into molecules, desorbing back into the plasma as the wall, and is saturated with the working gas. Here, the densities of recycling backscattered atoms and desorbed molecules decay with the distance from the wall because diverse elementary processes such as ionization, charge exchange and dissociation in the latter case, caused by collisions with the plasma electrons and ions, lead to disintegration of neutrals [11]. By the dissociation and ionization of molecules, the so-called Franck-Condon *fc* atoms are generated of a characteristic energy E_{fc} of 3.5 eV [3, 11]. By charge exchange collisions of the primary neutral species, listed above, with the plasma ions, *cx* atoms of higher energies and with chaotically oriented velocities are generated. Although, namely, the latter are of our particular interest, to describe them firmly, all the species introduced have to be considered. In the vicinity of a circular opening in the wall (see **Figure 1b**), any neutral particle is characterized by the components V_x and V_ρ of its velocity, where x and ρ are distances from the wall and opening axis (see **Figure 1b**).

2.1. Recycling molecules and atoms

Recycling species, lunched from the wall, comprise backscattered atoms and desorbed molecules. Henceforth, we assume that the x components of their velocities have single values $V_{bs,m}$ and distinguish two groups of particles moving outward and toward the opening axis, with $V_\rho = V_{bs,m}$ and $V_\rho = -V_{bs,m}$, correspondingly. The magnitudes of $V_{bs,m}$ are predefined by the generation mechanism for the species in question. Within the plasma the point with certain coordinates x and ρ can be reached only by particles, coming from the wall points $(0, \rho + x)$ for $V_\rho < 0$ and $(0, |\rho - x|)$ for $V_\rho > 0$, respectively. By taking into account the attenuation processes with neutrals in the plasma, one gets

$$n_{bs,m}(x,\rho) = \frac{n_{bs,m}(0,\rho+x) + n_{bs,m}(0,|\rho-x|)}{2} \exp\left(-\int_0^x \frac{\nu_{a,m}}{V_{bs,m}} dy\right) \tag{1}$$

where $\nu_a = n\left(k_{ion}^a + k_{cx}^a\right)$ and $\nu_m = n\left(k_{dis}^m + k_{ion}^m + k_{cx}^m\right)$ are the decay frequencies for atoms and molecules, correspondingly, with n being the plasma density assumed the same for electrons and ions, $k_{ion}^{a,m}$ are the rate coefficients of the ionization by electrons, $k_{cx}^{a,m}$ those for the charge exchange with ions, and k_{dis}^m that for the dissociation of molecules.

2.2. Franck-Condon (*fc*) atoms

The *fc* atoms are born by the destruction of molecules and have positive and negative values both of V_ρ and of V_x. Henceforth, we distinguish four groups of these species with the velocity components $\left(V_x, V_\rho\right) = \left(\pm V_{fc}, \pm V_{fc}\right)$, where $V_{fc} = \sqrt{E_{fc}/m}$ and m is the atom mass. The source density of *fc* atoms of each group is as follows:

$$S_{fc} = n\left(2k_{dis}^{m} + k_{ion}^{m} + k_{cx}^{m}\right)n_m/4$$

and depends on ρ through n_m. The particle densities $n_{fc\pm\pm}$, where the first subscript $\pm$ corresponds to the sign of V_x and the second one – of V_ρ, change along the characteristics $\pm x \mp \rho = const$ according to the continuity equation:

$$\sqrt{2}V_x \partial_l n_{fc\pm\pm} = S_{fc}(l) - \nu_a n_{fc\pm\pm}$$

where l is the length of the corresponding characteristics. The boundary conditions take into account that *fc* atoms are reflected with the probability R_{fc} from the wall, $x = 0$, and are absent far from the wall, $x \to \infty$. For the total density of *fc* atoms, $n_{fc} = n_{fc++} + n_{fc+-} + n_{fc-+} + n_{fc--}$, one can obtain

$$\begin{aligned} n_{fc}(x,\rho) = &\int_0^\infty \frac{S_{fc}(y,|\rho - x + y|) + S_{fc}(y,|\rho + x - y|)}{V_{fc}}\mu_0 dy + \\ &+ \frac{R_{fc}}{2}\Theta(\rho + x - \rho_0)\int_0^\infty \frac{S_{fc}(y,\rho + x + y) + S_{fc}(y,|\rho + x - y|)}{V_{fc}}\mu_1 dy + \\ &+ \frac{R_{fc}}{2}\Theta(|\rho - x| - \rho_0)\int_0^\infty \frac{S_{fc}(y,|\rho - x| + y) + S_{fc}(y,||\rho - x| - y|)}{V_{fc}}\mu_1 dy \end{aligned} \quad (2)$$

with

$$\mu_0 = \exp\left(-\frac{|U_x - U_y|}{V_{fc}}\right),\ \mu_1 = \exp\left(-\frac{U_x + U_y}{V_{fc}}\right),\ U_{x,y} = \int_0^{x,y} \nu_a dz,$$

the Heaviside function $\Theta(\xi \geq 0) = 1, \Theta(\xi < 0) = 0$ and ρ_0 being the opening radius (see **Figure 1b**).

2.3. Charge exchange *cx* atoms

The velocity distribution function of *cx* atoms, $f_{cx}(x,\rho,V_x,V_\rho)$, is governed by the kinetic equation:

$$V_x \partial_x f_{cx} + \frac{V_\rho}{\rho}\partial_\rho(\rho f_{cx}) = \frac{S_{cx}}{\pi V_{th}^2}\exp\left(-\frac{V_x^2 + V_\rho^2}{V_{th}^2}\right) - \nu_a f_{cx}, \quad (3)$$

Here, $S_{cx} = S_{cx}^0 + S_{cx}^1$ is the total density of the source of *cx* atoms, with $S_{cx}^0 = n\left[k_{cx}^m n_m + k_{cx}^a\left(n_{bs} + n_{fc}\right)\right]$ and $S_{cx}^1 = nk_{cx}^a n_{cx}$ being the contributions due to charge exchange collisions with ions of primary neutrals and *cx* atoms themselves, correspondingly, where

$$n_{cx} = \int_{-\infty}^{\infty} \int_{-\infty}^{\infty} f_{cx} dV_x dV_\rho;$$

is the density of the latter; the velocity distribution of the source is assumed as the Maxwellian one with the ion temperature T_i, and $V_{th} = \sqrt{2T_i/m}$ is the ion thermal velocity.

2.3.1. Integral-differential equations for the density of cx *atoms*

To solve Eq. (3), V_ρ is discretized as $\pm V_\rho^l$, with $V_\rho^l = \Delta V(l - 1/2)$, $\Delta V = V_{\max}/l_{\max}$, and $l = 1, \cdots, l_{\max}$. The V_x distribution functions $\varphi_l^\pm$ of particles with V_ρ in the range $\pm V_\rho^l - \Delta V/2 \leq V_\rho \leq \pm V_\rho^l + \Delta V/2$ are governed by the equations, following from the integration of Eq. (3) over these ranges:

$$V_x \partial_x \varphi_l^\pm \pm \frac{V_\rho^l}{\rho} \partial_\rho (\rho \varphi_l^\pm) = \frac{S_{cx} \delta_l}{2\sqrt{\pi} V_{th}} \exp\left(-\frac{V_x^2}{V_{th}^2}\right) - \nu_a \varphi_l^\pm, \tag{4}$$

with

$$\delta_l = \left\{ \operatorname{erf}\left[-\left(\frac{V_\rho^l + \Delta V/2}{V_{th}} \right) \right] - \operatorname{erf}\left[-\left(\frac{V_\rho^l - \Delta V/2}{V_{th}} \right) \right] \right\} / \operatorname{erf}\left(\frac{V_{\max}}{V_{th}} \right).$$

From the equation above, one gets the following ones for the variables $\varphi_l = \varphi_l^+ + \varphi_l^-$ and $\gamma_l = V_\rho^l (\varphi_l^+ - \varphi_l^-)$:

$$V_x \partial_x \varphi_l + \frac{1}{\rho} \partial_\rho (\rho \gamma_l) = \frac{S_{cx} \delta_l}{\sqrt{\pi} V_{th}} \exp\left(-\frac{V_x^2}{V_{th}^2}\right) - \nu_a \varphi_l, \tag{5}$$

$$\partial_x \gamma_l + \frac{\left(V_\rho^l\right)^2}{V_x \rho} \partial_\rho (\rho \varphi_l) = -\frac{\nu_a}{V_x} \gamma_l, \tag{6}$$

The latter equation is straightforwardly integrated with respect to x, and for the ρ-component of the flux density, one gets

$$\gamma_l = -\frac{\left(V_\rho^l\right)^2}{V_x \rho} \int_{x_0}^{x} \partial_\rho (\rho \varphi_l) \exp\left(\frac{U_y - U_x}{V_x} \right) dy.$$

Here, x_0 is the position, where the boundary condition is imposed; since there is no influx of *cx* atoms from the wall, $\gamma_l(x = 0) = 0$ for $V_x > 0$, neutral species are absent deep enough in the plasma and $\gamma_l(x \to \infty) \to 0$ for $V_x < 0$. The found expression for γ_l can be made more convenient if (i) the x-variation of terms involved is approximated by linear Taylor series:

$$\partial_\rho(\rho\varphi_l)(y) \approx \partial_\rho(\rho\varphi_l)(x) + \partial_x\partial_\rho(\rho\varphi_l)(x)\cdot(y-x),\ U_y \approx U_x + \nu_a(x)\cdot(y-x),$$

and (ii) by taking into account that the width of the region, occupied by *cx* atoms, is of several mean free path lengths (MFPL), that is, $|x-x_0| > |V_x|/\nu_a$ typically. As a result we get

$$\gamma_l \approx -(D_l/\rho)\times\partial_\rho(\rho\varphi_l),$$

with $D_l = \left(V_\rho^l\right)^2/\nu_a$.

By substituting the last expression into Eq. (5), this is reduced to the following one:

$$V_x\partial_x\varphi_l - \frac{D_l}{\rho}\partial_\rho^2(\rho\varphi_l) = \frac{S_{cx}\delta_l}{\sqrt{\pi}V_{th}}\exp\left(-\frac{V_x^2}{V_{th}^2}\right) - \nu_a\varphi_l. \tag{7}$$

Equation (7) can be integrated as the first-order equation with respect to x, with the boundary conditions similar to those for γ_l, that is, $\varphi_l(x=0)=0$ for $V_x>0$ and $\varphi_l(x\to\infty)\to 0$ for $V_x<0$. Finally, for the density of *cx* atoms within the range $V_\rho^l - \Delta V/2 \le |V_\rho| \le V_\rho^l + \Delta V/2$, $\eta_l = \int_{-\infty}^{\infty}\varphi_l dV_x$, one obtains the following integral-differential equation:

$$-\frac{D_l}{\nu_a\rho}\partial_\rho^2(\rho\eta_l) = \int_0^\infty \frac{S_{cx}\delta_l}{\sqrt{\pi}V_{th}}I_\alpha dy - \eta_l, \tag{8}$$

where $I_\alpha = \int_0^\infty F_\alpha du$, with $F_\alpha(u) = u^{-1}\exp(-u^2-\alpha/u)$ and $\alpha = |U_y - U_x|/V_{th}(y)$. For the total density of *cx* atoms, one has $n_{cx} = \sum_{l=1}^{l_{\max}}\eta_l$.

2.3.2. Diffusion approximation

By neglecting the ρ derivative and by considering a single V_ρ value, Eq. (8) is reduced to an integral one obtained in the 1D case (Eq. (16) in Ref. [6] or Eq. (11) in Ref. [4]). In this case $l\equiv 1$, $\delta_l = 1$ and $n_{cx} = \eta_1$. As it was demonstrated in Ref. [4], this integral equation can be reduced to an ordinary differential diffusion equation, if (i) the electron temperature is low enough and the ionization rate is much smaller than that of the charge exchange, $k_{ion}^a \ll k_{cx}^a$, and (ii) the characteristic dimension for the plasma parameter change is much larger than the typical MFPL for *cx* atoms V_{th}/ν_a. The same procedure can be performed in the case under the consideration, providing the following 2D diffusion equation:

$$-\frac{D_{th}}{\rho}\partial_\rho\left(\rho\partial_\rho n_{cx}\right) - \partial_x\left[\frac{\partial_x(n_{cx}T_i)}{\nu_a m}\right] = S_{cx}^0 - k_{ion}^a n n_{cx}, \tag{9}$$

with $D_{th} = V_{th}^2/(2\nu_a)$. The boundary conditions to Eq. (9) imply as follows: (i) *cx* atoms leave the plasma with the velocity close to the ion thermal one, and (ii) neutral species are absent far

from the wall, that is, $n_{cx}(x \to \infty) = 0$. Additionally, $\partial_\rho \eta_l = 0$ and $\partial_\rho n_{cx} = 0$ for $\rho = 0$ and $\rho \to \infty$ for Eqs. (8) and (9), respectively.

2.3.3. Assessment of the velocity space integral I_α

By inspecting Eq. (8), one can see the cause for large calculation time for kinetic computations for *cx* atoms. Even in the 1D case, for each grid point, one has to calculate enclosed double integrals over the ion velocity space and over the whole plasma volume, $0 \le y \le r_w$, and repeat this, in an iterative procedure, with respect to the whole profiles of $n_{cx}(x)$. In a 2D situation, the runs through the grid points in the (ρ, V_ρ) phase subspace are involved additionally into calculations. These can be, however, efficiently parallelized. The integral I_α is appeared due to the generation of *cx* atoms with the ion Maxwellian velocity distribution and consequent attenuation by ionization and *cx* collisions. With a high accuracy, it can be assessed by an approximate pass method [12]. The function $F_\alpha(u)$ is shown in **Figure 2a** for $\alpha = 0.3$, 1, and 3. One can distinguish four u intervals, where $F_\alpha(u)$ behaves principally differently: $u \le u_1$, $u_1 < u \le u_m$, $u_m < u \le u_2$, and $u_2 < u$. The characteristic points $u_{1,2}$ and u_m are defined by the conditions $F'_\alpha(u_m) = 0$ and $F''_\alpha(u_{1,2}) = 0$ for the derivatives $F'_\alpha = -F_\alpha g_1/u^2$ and $F''_\alpha = F_\alpha g_2/u^4$ with

$$g_1(u) = 2u^3 + u - \alpha, \quad g_2(u) = \left(g_1 + u\right)^2 - \left(2 + 6u^2\right)u^2.$$

For u_m one can use the Cardano formula for the real root of a cubic equation $u_m = \sqrt[3]{b+a} - \sqrt[3]{b-a}$ with $a = \alpha/4$ and $b = \sqrt{a^2 + 1/216}$. By searching for $u_{1,2}$, we notice that for the roots of interest the equation $g_2(u_{1,2}) = 0$ reduces to the following ones:

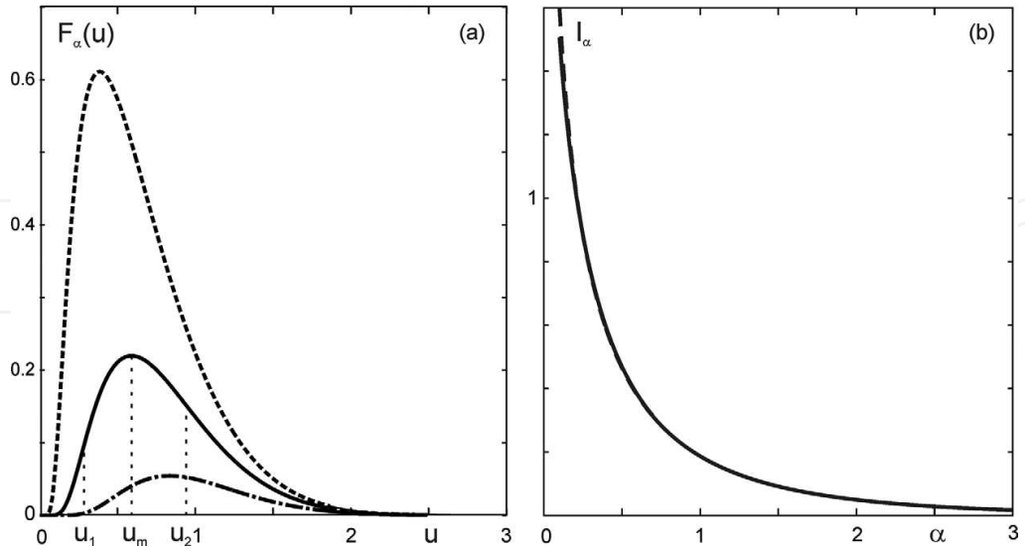

Figure 2. The functions $F_\alpha(u) = u^{-1}\exp\left(-u^2 - \alpha/u\right)$ for $\alpha = 1$ (solid curve), $\alpha = 0.3$ (dashed curve), and $\alpha = 3$ (dashed-dotted curve) (a); the integral $I_\alpha = \int_0^\infty F_\alpha(u)du$ estimated by the pass method (solid curve) and computed numerically (dashed curve) (b).

$$g_1(u_1) + u_1 + u_1\sqrt{2+6u_1^2} = 0, g_1(u_2) + u_2 - u_2\sqrt{2+6u_2^2} = 0.$$

With properly selected initial approximations accurate enough, solutions of these equations are found after three to five iterations with the Newton approach.

To assess the integrals I_α, we approximate function $F_\alpha(u)$ as a linear one at $u \le u_1$ and by polynomials of the fifth order at the intervals $u_1 < u \le u_m$ and $u_m < u \le u_2$. The coefficients are selected to reproduce $F_{\alpha m,1,2} = F_\alpha(u_{m,1,2})$, $F'_{\alpha 1,2} = F'_\alpha(u_{1,2})$, $F''_{\alpha m} = F''_\alpha(u_m)$, and $F'_\alpha(u_m) = F''_\alpha(u_{1,2}) = 0$. In addition, for $u > u_2$ the factor $\exp(-u^2)$ leads to a very fast decay of F_α with increasing u. Therefore, for the aim to assess the corresponding contribution to I_α, we approximate F_α by $\exp(-u^2 - \alpha/u_2)/u_2$. This results in the following expression:

$$I_\alpha \approx \frac{F_{\alpha 1}^2}{2F'_{\alpha 1}} + \frac{F_{\alpha 1}\delta_1 + F_{\alpha m}(u_2 - u_1) + F_{\alpha 2}\delta_2}{2} + \\ + \frac{F'_{\alpha 1}\delta_1^2 - F'_{\alpha 2}\delta_2^2}{10} + F''_{\alpha m}\frac{\delta_1^3 + \delta_2^3}{120} + \frac{\sqrt{\pi}}{2}\frac{1 - erfu_2}{u_2}\exp\left(-\frac{\alpha}{u_2}\right), \tag{10}$$

where $\delta_{1,2} = |u_m - u_{1,2}|$. **Figure 2b** shows I_α versus α found with the pass method, outlined above and evaluated numerically. By approximating the numerical results very accurately, the approximate pass method procedure allows to reduce the CPU time by a factor of 50 compared to direct estimates.

Alternatively to the usage of formula (10), one can calculate the integral I_α in advance and save the results in a table. Then, for any particular α, the integral I_α is interpolated from the values in this table. However, some time is needed to find the proper α interval, and this time grows up with $\alpha \to 0$ since $I_\alpha \to \infty$ as $-\ln\alpha$. Thus, the density of the data in the table has to be increased as $\alpha \to 0$, and it is not obvious that such a way is more time-saving than formula (10).

2.3.4. Numerical procedure

The procedure to solve Eq. (9) numerically is organized as follows: For the problem in question, with the plasma profiles assumed unaffected by the processes in the vicinity of the duct opening, the integral $I_\alpha(x, y)$ can be assessed once in advance. Then,

i. the source density $S_{cx}(x, \rho)$ is calculated, in the first approximation with $n_{cx} = 0$;

ii. for all x the first term on the right-hand side of the equation is computed as a function of ρ, and the second-order ordinary Eq. (8) is solved by the method outlined in [10] for all V_l;

iii. the next approximation for $n_{cx}(x, \rho)$ and $S_{cx}(x, \rho)$ is computed, and the procedure is repeated till the relative error in, for example, $n_{cx}(0, 0)$, becomes smaller than a desirable one.

A typical behavior of the error with the iteration number for calculations presented in the next section is shown in **Figure 3**. One can see that with consequent iterations the calculation error reduces steadily without any noise and the machine accuracy can be actually achieved.

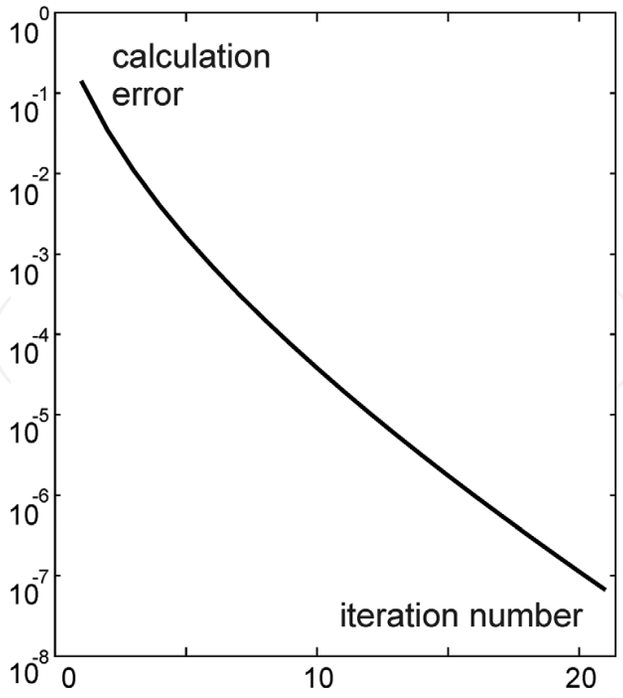

Figure 3. The reduction of the relative error in calculation with the iteration number.

Normally, a diffusion approximation is used to describe *cx* atoms to reduce CPU. The present approach to solve kinetic equation makes this unnecessary. To get the density of *cx* atoms, $n_{cx}(x,\rho)$, with a relative error below 10^{-6}, kinetic calculations require much less CPU time than it is needed to solve the diffusion equation. Thus, for 500 and 30 grid points in the x and ρ directions, respectively, $l_{\max}$ =10 and $V_{\max} = 3V_{th}$, the CPU times for a 1 GHz processor are 30 s and 112 min, correspondingly. Of course, the time for kinetic calculations increases significantly if neutrals affect the plasma background, and $I_\alpha(x,y)$ has to be evaluated by each iteration. Even in this case kinetic computations for *cx* atoms are done faster by factor of 4.

3. Results of calculations

Figure 4 shows the profiles of the plasma parameters, assumed homogeneous on the flux surfaces, across the surfaces, computed in [13] with the input parameters from the European DEMO project [1, 2]. The distance x from the first wall to a certain flux surface depends on the poloidal angle θ (see **Figure 1a**) and in **Figure 4** x corresponds to the torus outboard, $\theta = 0$, where this distance is minimal. The profiles of the *cx* atom density found with these parameters and for the duct radius $\rho_0 = 0.05\,\mathrm{m}$, at the opening axis, $\rho = 0$, and far from it, $\rho = 0.25\,\mathrm{m}$ are shown in **Figure 5**. There is a noticeable difference between the profiles of n_{cx} calculated in the diffusion approximation (5a) and kinetically (5b). In particular, the difference between the density profiles at these two positions is significantly larger in the diffusion approximation than for those computed kinetically.

http://dx.doi.org/10.5772/intechopen.76681

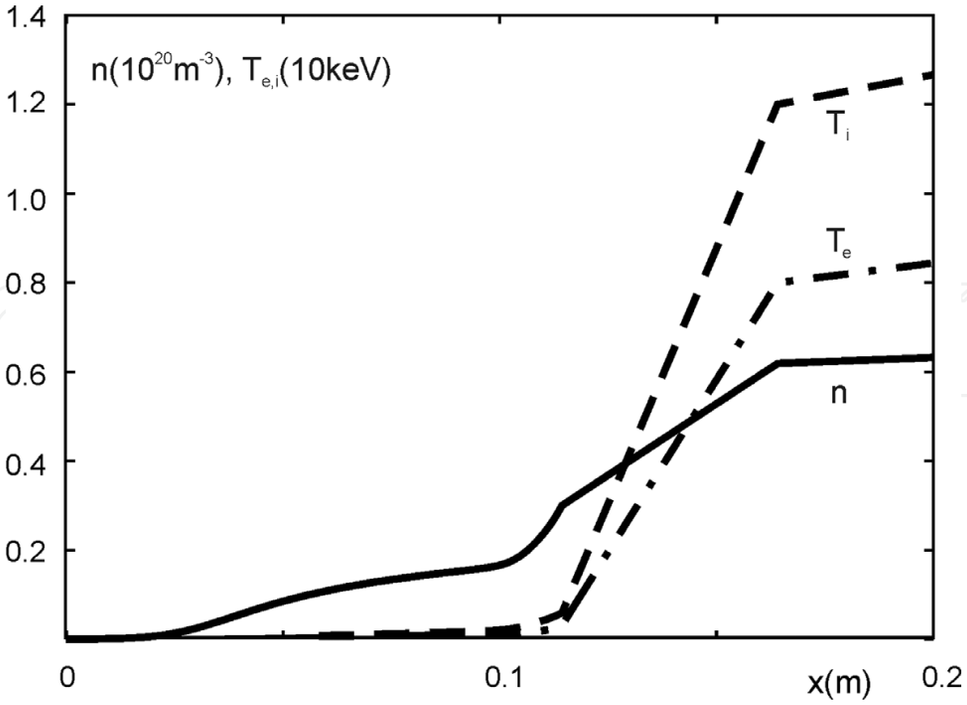

Figure 4. The profiles of the plasma density (solid curve), the ion (dashed curve), and electron (dashed-dotted curve) temperatures versus the distance from the wall at the DEMO torus outboard.

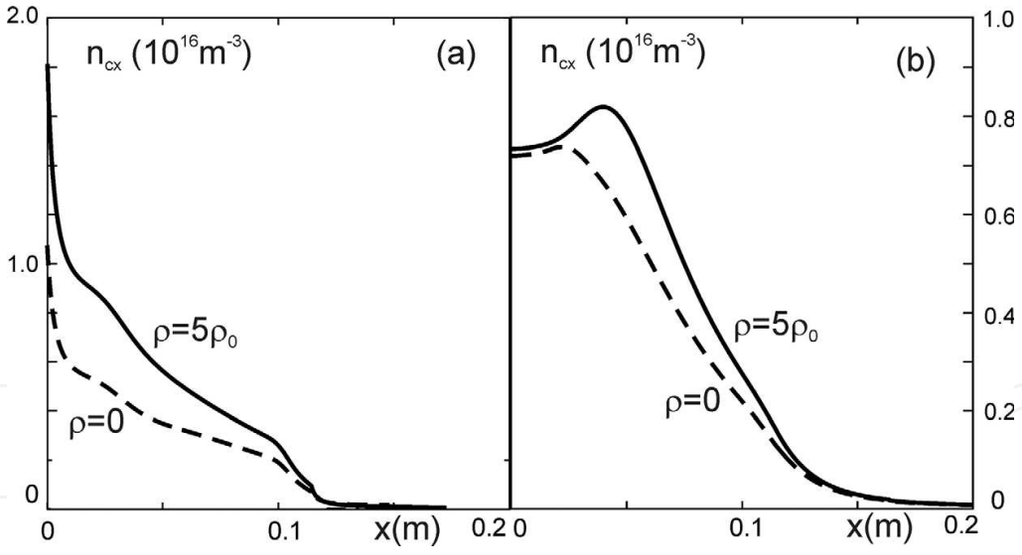

Figure 5. The profiles of the *cx* atom densities far from the opening (solid curve) and at its axis (dashed curve) computed in the diffusion approximation (a) and kinetically (b).

In the latter case, n_{cx} is still noticeable in much deeper and hotter plasma regions. This circumstance is of importance for the erosion of installations in ducts due to physical sputtering because this is very sensitive to the energy of impinging particles. To demonstrate this the erosion rate of a Mo mirror, imposed into the duct of three different radii ρ_0, at the distance h from its opening (see **Figure 1b**) is assessed. To do such assessment, consider an infinitesimally thin toroid within

the plasma, with a square cross section of the width $d\rho$, thickness dx, and the radius ρ, situated at the distance x from the wall. Cx atoms with the energies within the range E, $E + dE$ are generated in the toroid with the rate:

$$dR_{cx}(x,\rho,E) = S_{cx}(x,\rho)\varphi_i(x,E)2\pi\rho d\rho dx dE. \tag{11}$$

where

$$\varphi_i(x,E) = \frac{2\sqrt{E}}{\sqrt{\pi}T_i^{1.5}(x)}\exp\left[-\frac{E}{T_i(x)}\right]. \tag{12}$$

is the Maxwellian energy distribution function of ions.

Since cx atoms move in all directions, some of them hit the mirror inside the duct (see **Figure 1b**). Henceforth, we analyze the surface position at the duct axis. One can see that cx atoms generated only in toroids with $\rho \le \rho_{\max} = \rho_0(1 + x/h)$ can hit this mirror point. The contribution of the plasma volume in question to the density of the cx atom flux perpendicular to the mirror surface is

$$dj_{cx}(x,\rho,E) = dR_{cx}\frac{s\cdot\exp(-\lambda/s)}{4\pi\left[(x+h)^2+\rho^2\right]}, \tag{13}$$

where $s = \left[1+\rho^2/(x+h)^2\right]^{-1/2}$ is the cosine of the atom incidence angle with respect to the duct axis. The exponential factor in Eq. (13), with $\lambda(x,E) = U_x/\sqrt{2E/m}$, takes into account the destruction of cx atoms in ionization and charge exchange collisions on their way through the plasma. By ionization the atom disappears. By charge exchange a new cx atom is generated. The latter process is taken into account by the contribution S_{cx}^1 in the source density S_{cx}.

The energy spectrum of cx atoms, hitting the mirror, is characterized by their flux density $\gamma = \int dj_{cx}/dE$ in the energy range dE, where the integration is performed over ρ and x. By proceeding from ρ to s, according to the relation $\rho = (x+h)\sqrt{1/s^2-1}$, one gets

$$\gamma(h,\rho_0,E) = \int_0^{r_w}\varphi_i(x,E)dx\int_{h/\sqrt{h^2+\rho_0^2}}^{1}\frac{S_{cx}}{2}\exp\left(-\frac{\lambda}{s}\right)ds. \tag{14}$$

The density of the outflow of mirror particles eroded by physical sputtering with cx atoms is as follows:

$$\Gamma_{sp}(h,\rho_0) = \int_0^{\infty}dE\int_0^{r_w}\varphi_i(x,E)dx\int_{h/\sqrt{h^2+\rho_0^2}}^{1}\frac{S_{cx}}{2}\exp\left(-\frac{\lambda}{s}\right)Y_{sp}(E,s)ds \tag{15}$$

Here, Y_{sp} is the sputtering yield, whose dependence on E and s is calculated by applying semiempirical formulas from Ref. [14]. The erosion rate, measured henceforth in nm per

full-power year (nm/pfy), is $h_{sp} = \Gamma_{sp}/n_{sp}$, with the particle density of molybdenum n_{sp}. It is shown in **Figure 6** versus the distance h between the wall position and the mirror point in question. One can see that in the former case the erosion rate is by a factor of 2 larger than in the latter one. It is of importance to notice that h_{sp}, found with n_{cx} computed kinetically, does not unavoidably excides that obtained with n_{cx} calculated in the diffusion approximation. The results above have been gotten for a mirror positioned in a duct at the plasma outboard, that is, at the largest major radius R (see **Figure 1a**). Here, the local gradients of the plasma parameters are the largest because the distance between two particular flux surfaces has the minimum. Therefore, *cx* atoms penetrate, before they are ionized, into plasma regions with higher ion temperatures. The situation is different at the torus top where the corresponding distance has maximum and neutral species are attenuated already at significantly low n and T_i. This leads to noticeably smaller h_{sp} (see **Figure 7**). In this case, oppositely to the situation at the outboard, h_{sp} is larger if n_{cx} is computed in the diffusion approximation.

Due to technical requirements, an acceptable mirror erosion rate in a future fusion reactor should not exceed $1nm/pfy$. As one can see in the case of a duct at the torus outboard, this target level is exceeded significantly for all h and ρ_0 under consideration. Seeding of the working gas into the duct is considered as a possible way to diminish the erosion rate below the maximum level allowed. The energy of *cx* atoms, coming into the duct, is reduced through elastic collisions with gas molecules, before *cx* atoms hit the mirror. Elastic collisions between neutral species lead to scattering on large angles. Consider a *cx* atom which, without gas in the duct, can hit the mirror directly. If the gas is seeded, in a narrow duct in question, with $\rho_0 \ll h$, any collision of the *cx* atom with gas molecules leads to such a change of the atom velocity that with an overwhelming probability the atom will many times strike the duct wall before it gets the mirror. Through the collisions with the wall, the *cx* atom loses its energy so dramatically

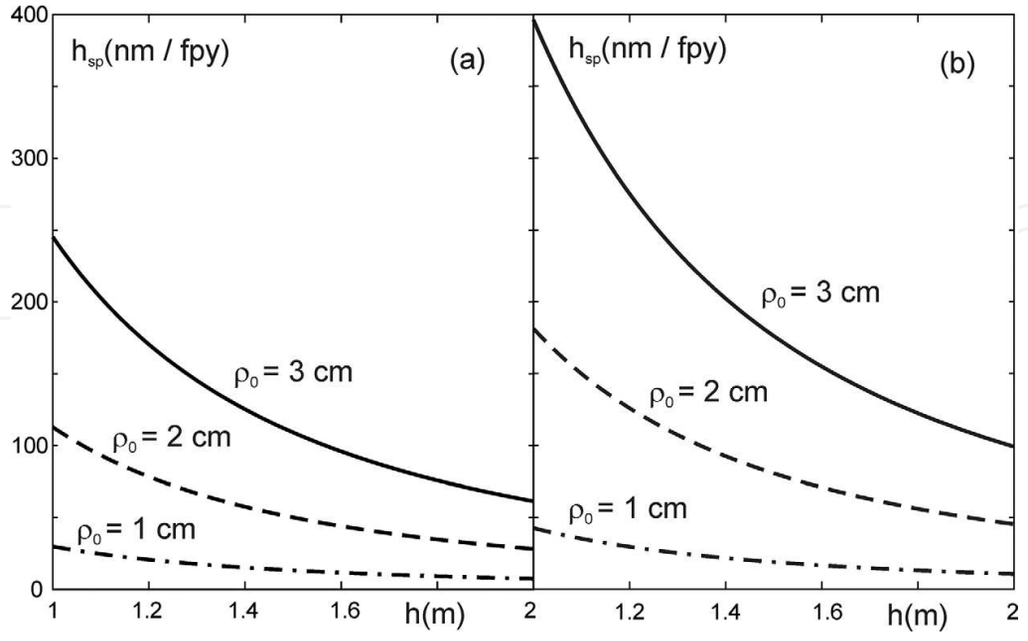

Figure 6. The erosion rate of a Mo mirror versus the distance from the wall position to the mirror surface for ducts positioned at the torus **outboard** computed with the density of cx atoms found in the diffusion approximation (a) and kinetically (b).

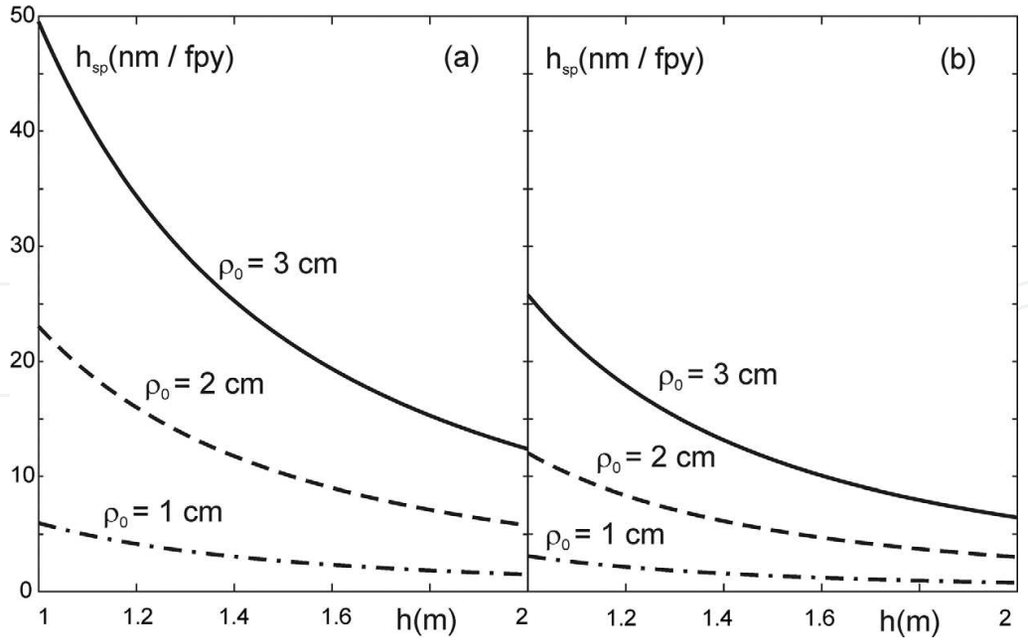

Figure 7. The erosion rate of a Mo mirror versus the distance from the wall position to the mirror surface for ducts positioned at the torus **top** computed with the density of *cx* atoms found in the diffusion approximation (a) and kinetically (b). (Note that the h_{sp} scale is different than in **Figure 6**).

that it cannot contribute to mirror erosion. The reduction of the flux j_E of incoming *cx* atoms with the energy E by collisions with the gas in the duct is governed by the equation:

$$dj_E/dl = -\sigma_{el}(E)n_g j_E,$$

where $\sigma_{el} \approx 3.8 \cdot 10^{-19} E^{-0.14} \left[m^2, eV\right]$ is the cross section for elastic collisions between *cx* atoms and molecules of hydrogen isotopes [15]. Consequently, the density of the outflow of mirror particles eroded by physical sputtering with *cx* atoms is modified, compared with Eq. (15), as follows:

$$\Gamma_{sp}(h,\rho_0) = \int_0^{\infty} dE \int_0^{r_w} \varphi_i dx \int_{h/\sqrt{h^2+\rho_0^2}}^{1} \frac{S_{cx}}{2} \exp\left(-\frac{\lambda + \sigma_{el} n_g h}{s}\right) Y_{sp}(E,s) ds \tag{16}$$

In **Figure 8**, the calculated dependences of the erosion rate h_{sp} on h and ρ_0 are shown for several magnitudes of the density n_g of the working deuterium gas in the mirror duct. One can see that the enhancement of n_g above a level of $2 \cdot 10^{19} \mathrm{m}^{-3}$ should lead to the reduction of h_{sp} below the target level of $1 nm/pfy$. The question, to what extent the local plasma parameters may be changed by the outflow of the gas from the duct, has to be investigated in the future on the basis of approaches developed in [16]. There, it has been demonstrated that the ionization of the gas outflowing into the SOL can lead to dramatic growth of the local density and cooling of the plasma to a temperature of 1 eV. Such cold dense plasma cloud can affect the transfer of *cx* atoms in the plasma near the opening in the wall.

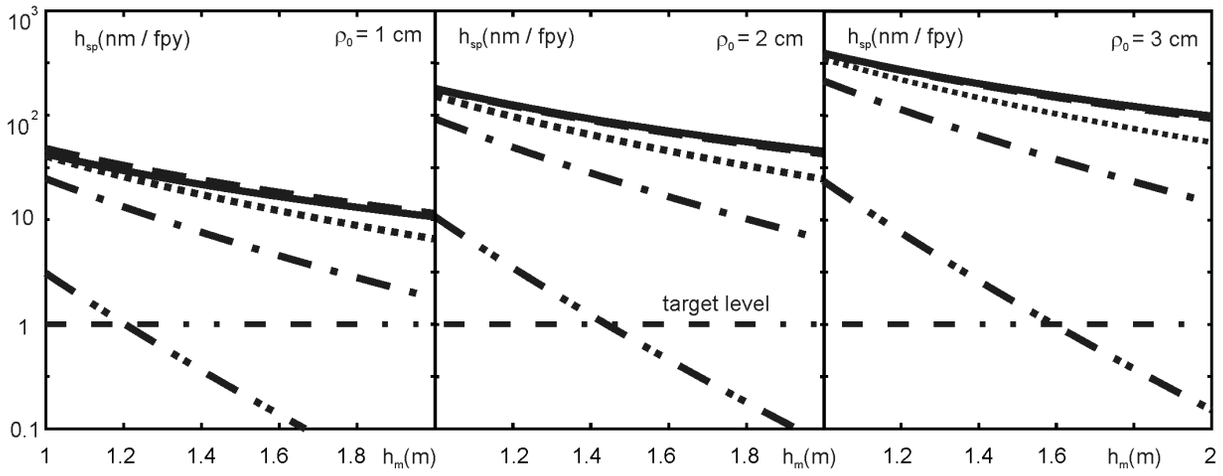

Figure 8. The erosion rate of a Mo mirror versus the distance from the wall position to the mirror surface for ducts positioned at the torus outboard computed with *cx* atoms treated kinetically for different gas densities in the duct: $n_g = 0$ (solid line), $3 \cdot 10^{17}\mathrm{m}^{-3}$ (dashed line), $3 \cdot 10^{18}\mathrm{m}^{-3}$ (dotted line), $10^{19}\mathrm{m}^{-3}$ (dashed-dotted line), and $3 \cdot 10^{19}\mathrm{m}^{-3}$ (dashed-double dotted line).

4. Conclusions

The iteration approach to solve 1D kinetic equation for *cx* atoms, proposed decades ago [6], has been elaborated further to describe the transport of these species in a 2D geometry, in the vicinity of a circular opening in the wall of a fusion reactor. Unlike the Monte Carlo methods, this approach does not generate statistical noise so that calculation errors can be reduced to the level restricted by the machine accuracy. In order to perform calculations for a broad range of input parameters and do a thorough comparison with the results, obtained in the diffusion approximation for *cx* atoms [13], the solving procedure has been accelerated by a factor of 50, by applying an approximate pass method to assess integrals in the velocity space from functions, involving the Maxwellian velocity distribution of plasma ions.

The found possibility to speed up kinetic calculations is of importance, in particular, to perform firm assessments of the erosion rate of the first mirrors in future fusion reactors like DEMO. For a mirror located at the torus outboard, more accurate kinetic calculations predict by a factor of 2 higher erosion rate than the approximate diffusion approach. The erosion rate can be reduced very strongly either by putting the mirror duct at the torus top or by seeding the working gas into the duct. In the latter case, the elastic collisions with molecules in the gas reduce significantly the fraction of *cx* atoms which can hit and erode the mirror.

Nomenclature

$D_{l,\,th}$	Diffusivity of *cx* atoms in kinetic and diffusion descriptions, correspondingly

E	Energies of ions and atoms
$F_\alpha(u) \equiv \frac{1}{u}\exp\left(-u^2 - \frac{\alpha}{u}\right), I_\alpha \equiv \int_0^\infty F_\alpha[u]du$	
h	Distance from duct opening to the mirror
h_{sp}	Mirror erosion rate in *nm* per full-power year
$\gamma(h, \rho_0, E)$	Flux density of *cx* atoms onto the mirror
$\Gamma(h, \rho_0)$	Outflow density of sputtered mirror particles
$k_{cx}^{a,m}$	Charge exchange rate coefficients
k_{dis}^{m}	Molecule dissociation rate coefficient
$k_{ion}^{a,m}$	Ionization rate coefficients
$\lambda(x, E) = U_x/\sqrt{2E/m}$	
m	Mass of atoms
n	Plasma density
$n_{m,bs,fc,cx}$	Densities of different neutral species—desorbed molecules, backscattered atoms, Franck-Condon, and charge exchanged atoms, respectively
$\nu_{m,a}$	Decay frequencies for molecules and atoms
$R_{cx}(x, \rho, E)$	The generation rate of *cx* atoms in the energy range $E, E + dE$ within an infinitesimally thin plasma toroid of the width $d\rho$, thickness dx, the radius ρ, and situated at the distance x from the wall
ρ	Distance from the opening axis
ρ_0	The opening radius
s	Cosine of the *cx* atom incidence angle with respect to the duct axis
$S_{fc,cx}$	Source densities of *fc* and *cx* atom species
$S_{cx}^{0,1}$	*cx* atom source density contributions due to charge exchange of primary neutral species and *cx* atoms
σ_{el}	Cross section for elastic collisions between *cx* atoms and molecules of hydrogen isotopes
$T_{e,i}$	Electron and ion temperatures
$U_{x,y} \equiv \int_0^{x,y} \nu_a dz$	

$V_{m,bs,fc}$	Absolute velocities of neutral species
$V_{x,\rho}$	Velocity components perpendicular to the wall and to the opening axis, respectively
$V_{th} = \sqrt{2T_i/m}$	Thermal velocity of ions
$\varphi_i(x,E)$	Energy distribution function of ions
x	Distance from the wall

Author details

Mikhail Tokar

Address all correspondence to: m.tokar@fz-juelich.de

Institute for Energy and Climate Research – Plasma Physics (IEK-4), FZJ, Jülich, Germany

References

[1] Federici G, Kemp R, Ward D, Bachmann C, Franke T, Gonzalez S, Lowry C, Gadomska M, Harman J, Meszaros B, Morlock C, Romanelli F, Wenninger R. Mint: Overview of EU DEMO design and R&D activities. Fusion Engineering and Design. 2014;**89**:882-889. DOI: 10.1016/j.fusengdes.2014.01.070

[2] Wenninger R, Arbeiter F, Aubert J, Aho-Mantila L, Albanese R, Ambrosino R, Angioni C, Artaud JF, Bernert M, Fable E, Fasoli A, Federici G, Garcia J, Giruzzi G, Jenko F, Maget P, Mattei M, Maviglia F, Poli E, Ramogida G, Reux C, Schneider M, Sieglin B, Villone F, Wischmeier M, Zohm H. Mint: Advances in the physics basis for the European DEMO design. Nuclear Fusion. 2015;**55**:063003. DOI: 10.1088/0029-5515/55/6/063003

[3] Stangeby PC. The Plasma Boundary of Magnetic Fusion Devices. Bristol and Philadelphia: Institute of Physics Publishing; 2000. p. 717. ISBN: 0 7503 0559 2

[4] Tokar MZ. Mnt: Scrape-off layer modeling with kinetic or diffusion description of charge-exchange atoms. Physics of Plasmas. 2016;**23**:122512. DOI: 10.1063/1.4972538

[5] Landau DP, Binder K. A Guide to Monte Carlo Simulations in Statistical Physics. Cambridge: University Printing House; 2015. p. 519. ISBN: 9781107074026

[6] Rehker S, Wobig H. Mint: A kinetic model for the neutral gas between plasma and wall. Plasma Physics. 1973;**15**:1083-1097

[7] Rognlien TD, Brown PN, Campbell RB, Kaiser TB, Knoll DA, McHugh PR, Porter GD, Rensink ME, Smith GR. Mint: 2-D Fluid transport simulations of gaseous/radiative divertors. Contributions to Plasma Physics. 1994;**34**:362-367

[8] Weber S. Mint: Aiming at 3-dimensional plasma fluid modelling of the W7-X divertor. Contributions to Plasma Physics. 1998;**38**:43-48

[9] Tokar MZ, Beckers M, Biel W. Mint: Erosion of installations in ports of a fusion reactor by hot fuel atoms. Nuclear Materials and Energy. 2017;**12**:1298-1302. DOI: 10.1016/j.nme.2017.01.006

[10] Tokar MZ. Mint: Modelling of profile evolution by transport transitions in fusion plasmas. In: Ahsan A, editor. Two Phase Flow, Phase Change and Numerical Modeling. Rijeka: InTech; 2011. pp. 149-172. ISBN: 978-953-307-584-6

[11] Janev RK, Langer WD, Evans KJ, Post DEJ. Mint: Elementary Processes in Hydrogen-Helium Plasmas. Hamburg: Springer; 1987. p. 328. ISBN: 978-3-642-71935-6

[12] Mathews J, Walker RL. Mint: Mathematical Methods of Physics. 2nd ed. Menlo Park: Benjamin; 1970. p. 515. ISBN: 0805370021

[13] Tokar MZ. Mint: An assessment for the erosion rate of DEMO first wall. Nuclear Fusion. 2018;**58**:016016. DOI: 10.1088/1741-4326/aa92dd

[14] Eckstein W, García-Rosales C, Roth J, Ottenberger W. Mint: Sputtering data. Garching: Institute of Plasma Physics; IPP 9/82 [Internet]. 1993. Available from: http://pubman.mpdl.mpg.de/pubman/item/escidoc:2131245:1/component/escidoc:2131244/IPP 9 82.pdf

[15] McGuire P, Krüger H. Mint: Elastic and rotationally inelastic H-H2 and H-D2 collisions. The Journal of Chemical Physics. 1975;**63**:1090-1094

[16] Tokar MZ. Mint: Modeling of localized impulsive injection of neutrals and plasma response. Plasma Physics and Controlled Fusion. 2017;**59**:055005-055012. DOI: 10.1088/1361-6587/aa6219